Krauskopf, B., & Osinga, HM. (2006). *Visualization of geodesic level sets on global manifolds*. http://hdl.handle.net/1983/878

Early version, also known as pre-print

## University of Bristol - Explore Bristol Research
### General rights

# Visualization of geodesic level sets on global manifolds

Bernd Krauskopf[1] and Hinke M Osinga[1]

Bristol Centre for Applied Nonlinear Mathematics, Department of Engineering Mathematics, University of Bristol, Bristol BS8 1TR, United Kingdom
b.krauskopf@bristol.ac.uk, h.m.osinga@bristol.ac.uk

**Summary.** If one wants to study the global dynamics of a given system, key components are the stable or unstable manifolds of invariant sets, such as equilibria and periodic orbits. Even in the simplest examples, these global manifolds must be approximated using numerical computations. We discuss an algorithm for computing global manifolds of vector fields that is decidedly geometric in nature. A two-dimensional manifold is built up as a collection of approximate geodesic level sets, i.e. topological circles. Our method allows to visualize the resulting surface by making use of the geodesic parametrization. This is a big advantage when one wants to understand the geometry of complicated two-dimensional manifolds, as is illustrated with examples in three- and four-dimensional vector fields.

## 1 Introduction

We are concerned here with the problem of understanding the global behavior of a dynamical system that is defined by a set of ordinary differential equations. Written in the form of a vector field, the system takes the general form

$$\dot{\mathbf{x}} = \mathbf{f}(\mathbf{x}, \lambda), \tag{1}$$

where $\mathbf{x}$ is a point from an $n$-dimensional phase space $\mathbf{X}$, $\lambda$ is a multi-dimensional parameter, and $\mathbf{f}$ is a sufficiently smooth (say, twice differentiable) vector-valued function. Indeed countless mathematical models arising in applications can be represented in this general framework; see, for example, [GH86, St94] as general entry points to the dynamical systems literature. As specific examples we will consider below the well-known Lorenz system, which has a three-dimensional phase space, and a model for the controlled inverted planar pendulum, which has a four-dimensional phase space.

In order to understand the bahavior of the system, one first considers the equilibria of (1), which are the points where $\mathbf{f}(\mathbf{x}, \lambda) = 0$. An equilibrium is typically either an attractors, a repellor or a saddle point, depending on

whether the eigenvalues of the linearization $\mathbf{Df}$ at the equilibrium have exclusively negative real parts, exclusively positive real parts, or are a mix of both, respectively. (Typical means here that there are no eigenvalues with zero real part.) The crucial role for organising the overall or global dynamics is played by the saddle points. Namely, a saddle point $\mathbf{x}_0$ comes with a stable manifold $W^s(\mathbf{x}_0)$ and an unstable manifold $W^u(\mathbf{x}_0)$, which are defined as the sets of all points in the phase space $\mathbf{X}$ that converge to $\mathbf{x}_0$ in forward and backward time, respectively. According to the Stable Manifold Theorem [PdM82] these sets are actually smooth immersed manifolds that are tangent to (and of the same dimension as) the stable and unstable eigenspaces. The importance of these manifolds for the overall dynamics essentially lies in two facts. First of all, stable manifolds often act as boundaries of basins of attraction and, secondly, intersections of $W^s(\mathbf{x}_0)$ and $W^u(\mathbf{x}_0)$ are associated with chaotic dynamics.

The computation of global invariant manifolds in dynamical systems is an active field of research. The difficulty is that these objects are not given in the form of an implicit equation. Therefore, they need to be 'grown' by starting from local information, for example, near the saddle point. This is a nontrivial task already for manifolds of dimension two, which is the case considered here. Several methods are available today to compute global invariant manifolds (mostly of dimension two); see the recent survey [KOD+05]. Regardless of the choice of method to use, one is faced with the problem of visualizing the resulting surfaces in an efficient manner in order to extract the information on the global dynamics of the system.

In this paper we demonstrate with two examples the opportunities for the visualization of complicated two-dimensional manifolds afforded by our own method. The key here is that our method computes a global invariant manifold in a very geometrical way, namely by building it up step by step as a set of geodesic levels; sets [KO03, EKO07] for details. The method can be used for calculating manifolds of arbitrary dimension that are associated with arbitrary compact invariant objects, like equilibria, periodic orbits, or higher-dimensional normally hyperbolic manifolds. Since we only shows two-dimensional stable manifolds of saddle points in our examples, let us explain how the method works for this case. A computation starts from a small disk in the stable eigenspace of the saddle point; its boundary is the first geodesic level set, which is a circle represented by a regular mesh. At every step a new geodesic level set (a topological circle) is added at a distance that is governed by the local curvature of the manifold along geodesics. The new geodesic level set is constructed pointwise by solving a two-point boundary value problem. Mesh points are added or removed on the new geodesic level set as appropriate to guarantee a uniform bound on the mesh quality. When the entire new geodesic level set has been found, a triangulated band between the new and last geodesic level set is added to the mesh representation of the surface. The computation stops when a pre-specified geodesic distance has been reached.

The result is a natural and geometric representation of the manifold in terms of a geodesic mesh that consists locally near each mesh point of a near perpendicular intersection of approximate geodesic level sets and approximate geodesics. It is this property that we exploit in the visualizations presented here. Namely, in Sect. 2 we show the two-dimensional manifold of the origin of the three-dimensional Lorenz system, and in Sect. 3 we visualize a two-dimensional manifold in the four-dimensional phase space of a controlled inverted pendulum. We used Geomview [PLM93] for the rendering of the manifolds.

## 2 Visualizing the Lorenz manifold

The Lorenz system was derived by Edward Lorenz in the 1960s as a very simplified model of Rayleigh-Bénard convection in the atmosphere. They can be written in the form (1), namely as the vector field

$$\begin{cases} \dot{x} = \sigma(y - x), \\ \dot{y} = \varrho x - y - xz, \\ \dot{z} = xy - \beta z, \end{cases} \tag{2}$$

which has the three-dimensional phase space $\mathbb{R}^3$. For the now classic choice of the parameters $\sigma = 10$, $\varrho = 28$, and $\beta = \frac{8}{3}$ Lorenz found sensitive dependence on the initial condition and the now famous Lorenz attractor [Lo63].

In this section we consider the stable manifold $W^s(\mathbf{0})$ of the origin, which is a saddle point with one unstable and two stable eigenvalues. Hence, $W^s(\mathbf{0})$ is a two-dimensional smooth surface. Geometrically, it divides points that initially go to one or the other 'wing' of the Lorenz attractor. More generally, $W^s(\mathbf{0})$ organises the chaotic dynamics of the Lorenz system in a global way, which is why we refer to it as the *Lorenz manifold*; see [OK02, KO04] and also the companion paper [OKD07].

Figure 1 shows the Lorenz manifold $W^s(\mathbf{0})$ computed up to geodesic distance 151.75; the origin $\mathbf{0}$ is in the middle of the images and the vertical axis is the $z$-axis, which is invariant under (2). Note further that, due to the symmetry $(x, y) \mapsto (-x, -y)$ of the Lorenz system, $W^s(\mathbf{0})$ is symmetric under a rotation by $\pi$ about the $z$-axis. The Lorenz manifold is rendered transparent in Fig. 1 so that its 'internal' structure can be seen. The first feature one notices is the main helix of $W^s(\mathbf{0})$ around the positive $z$-axis. Notice also the two secondary (and symetrically related) helices near the main helix. These helices arise because $W^s(\mathbf{0})$ spirals around two smooth symmetrical curves (the one-dimensional stable manifolds of a symmetric pair of nontrivial saddle points) in opposite directions.

Even when it is rendered transparent it is not easy to understand the intricate geometry of $W^s(\mathbf{0})$ near the origin. To help with the visualization we move a geodesic band of a different color over the surface; it is shown in
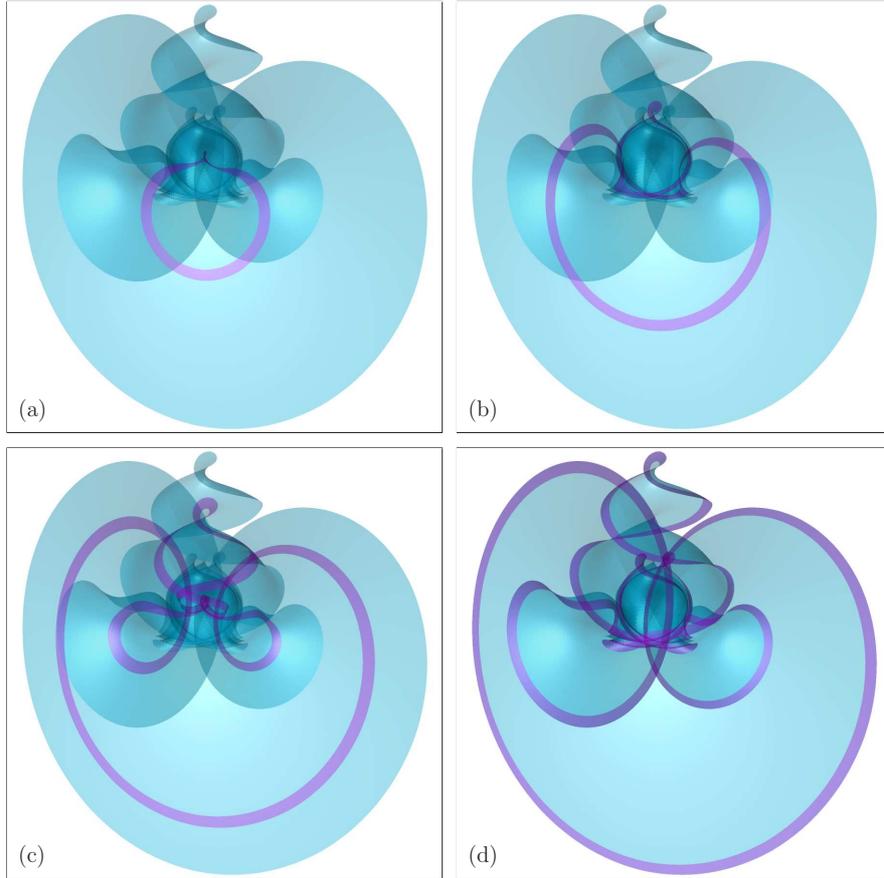
**Fig. 1.** The Lorenz manifold $W^s(\mathbf{0})$ of system (2) computed up to geodesic distance 151.75 and rendered transparent. To bring out its complicated geometry, a differently colored transparent geodesic band is moved over the surface; shown is the band covering geodesic distances 38.75–46.75 (a), 74.75–82.75 (b), 110.75–118.75 (c), and 144.75–151.75 (d).

four different positions in Fig. 1. A band near the origin is small and almost perfectly round. For increasing geodesic distance from the origin the band starts to pick up the spiralling along the main helix; see panel (a). It then spirals more near the origin and simultaneously moves up the main helix; see panels (b) and (c). For even larger geodesic distances this results in the creation of the two secondary helices on the band, as is illustrated in Fig. 1(d) with the outer most band of the computed surface.

It is important to realise that each geodesic band is unknotted. This corresponds to the fact that the Lorenz manifold itself is topologically simply a disk. The geodesic mesh representation of $W^s(\mathbf{0})$ that we compute can be

interpreted as an illustration of an (unknown) smooth map that embeds the standard disk into $\mathbb{R}^3$. As is clear from Fig. 1, such an embedding can be very complicated. We finally remark that the geodesic mesh computed by our method translates naturally into crochet instruction, which allowed us to make a real model of the Lorenz manifold; see [OK04] for details and images of the crocheted Lorenz manifold.

## 3 Visualizing a 2D manifold in four dimensions

As an example of a four-dimensional system with a two-dimensional stable manifold of physical relevance we consider an inverted planar pendulum that is balanced on a cart subject to a horizontal control force [HO2001, JYH99, OH06], which can be written as

$$\ddot{x}_1 = \frac{\frac{g}{l}\sin(x_1) - \frac{1}{2}m_r x_2^2 \sin(2x_1) - \frac{m_r}{m\,l} cos(x_1)\,u}{\frac{4}{3} - m_r \cos^2(x_1)}. \tag{3}$$

Here $x_1$ is the angle measured from the upright position (not taken modulo $2\pi$) and $x_2 = \dot{x}_1$ is its angular velocity, $m_r$ is the mass fraction of the pendulum with respect to the total mass (of pendulum and cart), $l$ is the length of the pendulum, and $g$ is the Earth's gravitational constant. The function $u$ constitutes a control that is supposed to stabilize the point $(x_1, x_2) = (0, 0)$, an unstable equilibrium corresponding to the upright position.

We associate a cost with the stabilization via the instantaneous cost function

$$Q(x_1, x_2, u) = \mu_1 x_1^2 + \mu_2 x_2^2 + \mu_3 u^2 \tag{4}$$

that penalizes both the state and the control, as long as the origin is not stablized. Here $\mu_1$, $\mu_2$ and $\mu_3$ are positive parameters. Pontryagin's maximum principle [vdS94] ensures that an optimal control $u$ exists that minimizes the cost function $Q$ over the infinite time interval $[0, \infty)$. The optimal solution is represented by points on the two-dimensional stable manifold $W^s(\mathbf{0})$ of the four-dimensional vector field given by the Hamiltonian

$$H(x_1, x_2, p_1, p_2) = Q(x_1, x_2, u^*(x_1, x_2, p_1, p_2)) + p_1 x_2 +$$
$$p_2\,f(x_1, x_2) + p_2\,c(x_1, x_2)\,u^*(x_1, x_2, p_1, p_2) \tag{5}$$

where $u^*(x_1, x_2, p_1, p_2) = -\frac{1}{2\mu_3}\,c(x_1, x_2)p_2$. Namely, for any given initial condition $(x_1, x_2, p_1, p_2)$ on $W^s(\mathbf{0})$, the projection of the corresponding trajectory onto the $(x_1, x_2)$-plane corresponds to a stabilizing solution via the (implicitly defined) feedback control $u = u^*(x_1, x_2, p_1, p_2)$ that locally minimizes (4). Indeed, if in this projection $W^s(\mathbf{0})$ covers a point $(x_1, x_2)$ more than once, then typically only one of these solutions is optimal and the others are only suboptimal; see [HO2001, OH06] for more details.
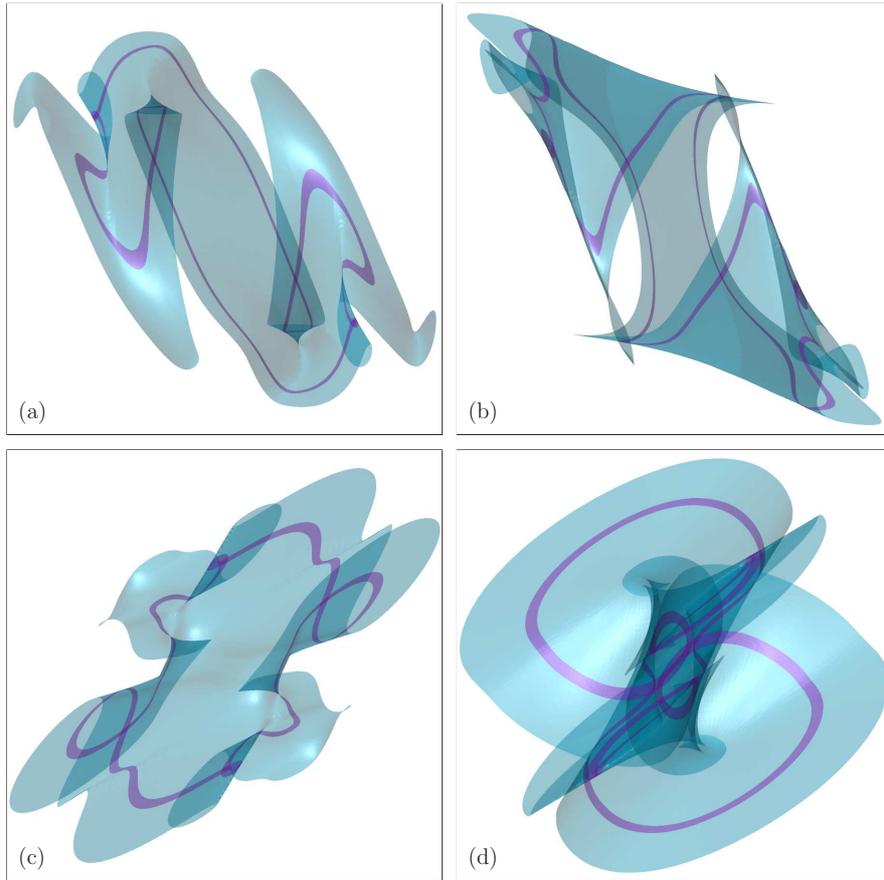
**Fig. 2.** The two-dimensional stable manifold $W^s(\mathbf{0})$ in $(x_1, x_2, p_1, p_2)$-space of the controlled inverted pendulum (5). The surface is rendered transparent and is shown simultaneously in the four projections $p_2 = 0$ (a), $p_1 = 0$ (b), $x_2 = 0$ (c), and $x_1 = 0$ (d); the differently colored band covers geodesic distances 19.0–20.0.

Figure 2 shows $W^s(\mathbf{0})$ for the parameters in [JYH99], namely $m_r = 0.2$, $l = 0.5\,\mathrm{m}$, and cost function parameters $\mu_1 = 0.1$, $\mu_2 = 0.05$ and $\mu_3 = 0.01$. The two-dimensional manifold $W^s(\mathbf{0})$ was computed up to a geodesic distance of approximately 26.25. It is rendered transparent in Fig. 2 and shown as four projections onto the three-dimensional subspaces that one obtains by setting one of the coordinates to zero. The transparent rendering allows one to see how $W^s(\mathbf{0})$ 'sits' in each of the three-dimensional projections. As with the previous example, we used our method for the computation of $W^s(\mathbf{0})$. Hence, the computed part of $W^s(\mathbf{0})$ is again a topological disk that is parametrized by the geodesic level sets. In particular, the boundary of the computed manifold

has the same geodesic distance to the origin, which lies in the centre of the manifold.

We can further help with the interpretation of the geometry of $W^s(\mathbf{0})$ in $\mathbb{R}^4$, by moving a geodesic band over it and observe how its geometry changes as it moves simultanously in all four projections. The differently colored band illustrated in Fig. 2 is the geodesic band covering the range 19–20. Note that this band divides the manifold $W^s(\mathbf{0})$ into an inner disk and an outer annulus, which is not at all obvious in Fig. 2(d).

## 4 Conclusions

The computation of (un)stable manifolds is an important tool when one wants to obtain a global understanding of how the dynamics of a vector field is organized. Particularly in the presence of chaotic dynamics, the geometry of global invariant manifolds can be very complicated, so that an appropriate visualization is a necessity.

We demonstrated here how the geodesic mesh representation that is the result of our method in [EKO07, KO03] can be used to visualize the geometry of a global manifold. In particular the technique of moving a differently colored geodesic band over the manifold adds an new dimension to the visualization. This is especially useful when one is confronted with the problem of understaning the geometry of a two-dimensional surface in an ambient space of dimension larger than three.

## References

[EKO07]  England, J.P., Krauskopf, B., Osinga, H.M.: Computing two-dimensional global invariant manifolds in slow-fast systems. Int. J. Bifurcation and Chaos, **17**(3) (2007) (in press)

[GH86]  Guckenheimer, J., Holmes, P.: Nonlinear Oscillations, Dynamical Systems and Bifurcations of Vector Fields. 2nd Printing, Springer-Verlag, New York (1986)

[HO2001]  Hauser, J. and Osinga, H.M.: On the geometry of optimal control: the inverted pendulum example. In: Proceedings of the American Control Conference Vol. 2, Arlington, VA, pp. 1721–1726 (2001)

[JYH99]  Jadbabaie, A., Yu, J. and Hauser, J.: Unconstrained receding horizon control: stability and region of attraction results. IEEE Trans. Automat. Control, **46**,776–783 (1999)

[KO03]  Krauskopf, B., Osinga, H.M.: Computing geodesic level sets on global (un)stable manifolds of vector fields. SIAM J. Appl. Dyn. Sys., **4**(2), 546–569 (2003)

[KO04]  Krauskopf, B., Osinga, H.M.: The Lorenz manifold as a collection of geodesic level sets. Nonlinearity **17**(1), C1–C6 (2004)

[KOD+05]  Krauskopf, B., Osinga, H.M., Doedel, E.J., Henderson, M.E., Guck-
          enheimer, J., Vladimirsky, A., Dellnitz, M., Junge, O.: A survey of
          methods for computing (un)stable manifolds of vector fields. Int. J.
          Bifurcation and Chaos **15**(3), 763–791 (2005)
[Lo63]    Lorenz, E.N.: Deterministic nonperiodic flows. J. Atmospheric Sci., **20**,
          130–141 (1963)
[OH06]    Osinga, H.M., Hauser, J.: The geometry of the solution set of nonlin-
          ear optimal control problems. J. Dynamics and Differential Equations,
          **18**(4), 881–900 (2006)
[OK02]    Osinga, H.M., Krauskopf, B.: Visualizing the structure of chaos in the
          Lorenz system. Computers and Graphics, **26**(5), 815–823 (2002)
[OK04]    Osinga, H.M., Krauskopf, B.: Crocheting the Lorenz manifold. Math.
          Intelligencer, **26**(4), 25–37 (2004)
[OKD07]   Osinga, H.M., Krauskopf, B., Doedel, E.J.: Visualizing the transition
          to chaos in the Lorenz system. This volume (2007)
[PdM82]   Palis, J., de Melo, W.: Geometric Theory of Dynamical Systems.
          Springer, New York (1982)
[PLM93]   Phillips, M., Levy, S., Munzner, T.: Geomview: An Interactive Geome-
          try Viewer. Notices of the American Mathematical Society, **40**: 985–988
          (1993); This software and the accompanying manual are available at
          `http://www.geom.uiuc.edu/` (accessed November 2006).
[vdS94]   Schaft, A.J. van der: $L_2$-Gain and Passivity Techniques in Nonlin-
          ear Control Lecture Notes in Control and Information Sciences **218**,
          Springer, Berlin (1994)
[St94]    Strogatz, S.: Nonlinear Dynamics and Chaos. Addison Wesley, Boston,
          MA (1994)